

Computer Programs in Physics

HYPIC: A fast hybrid EM PIC-MCC code for ion cyclotron resonance energization in cylindrical coordinate systemMingyang Wu (吴明阳), Andong Xu (许安冬), Chijie Xiao (肖池阶)^{*}

State Key Laboratory of Nuclear Physics and Technology, School of Physics, Fusion Simulation Center, Peking University, Beijing 100871, China

ARTICLE INFO

Edited by David W. Walker

Program summary

Program title: HYPIC

Licensing provisions: BSD 3-clause

Programming language: Fortran

Nature of problem: The code solves the electromagnetic field distribution in wave-plasma interactions and the motion of ions in the presence of electrostatic, electromagnetic, background magnetic fields, and collisions in two-dimensional (2D) (r, z) cylindrical coordinate system. The code is able to fast simulate the antenna-plasma interactions, ion cyclotron resonance energization and/or ion cyclotron resonance heating processes in linear devices, such as high-power electric propulsion, magnetic mirror, and field-reversed-configuration, etc.

Solution method: The PIC method with adiabatic electrons is used to fast simulate of the motion of ions by 4-stage Runge–Kutta time integral. The frequency-domain finite-difference method to solve Maxwell's equations allows for a fast solution of radio-frequency wave-plasma interactions. Monte Carlo collisions are used to deal with collisions of electrons and ions.

Additional comments including restrictions and unusual features: The current version only supports solving axisymmetric 2D problems.

Keywords:

Ion cyclotron resonance heating
Ion cyclotron resonant energization
Particle in cell
High-power electric propulsion
Magnetic mirror

ABSTRACT

Ion cyclotron resonance energization (ICRE) such as ion cyclotron resonance heating (ICRH) is widely applied to magnetic confinement fusion and high-power electric propulsion. Since ICRE involves cyclotron resonance processes, a kinetic model is required. Both conventional particle-in-cell (PIC) simulations and solving the Boltzmann equation require enormous computation and memory. The hybrid simulation incorporating of adiabatic electrons and PIC ions provides a viable solution for both a substantial reduction in computation and the inclusion of cyclotron resonance effects. Under the adiabatic electron approximation, we have developed a two-dimensional (r, z) hybrid electromagnetic (EM) PIC-MCC (Monte-Carlo collision) simulation program, named HYPIC. The advantages of HYPIC are the inclusion of ion kinetic effects, electrostatic (ES) and EM effects, and collisional effects of ions and electrons, with a small computation. The HYPIC program is able to fast simulate the antenna-plasma interactions and the ion cyclotron resonance energization and/or ion cyclotron resonance heating processes in linear devices, such as high-power electric propulsion, magnetic mirror, and field-reversed-configuration (FRC), etc.

1. Introduction

Ion cyclotron resonance energization (ICRE) such as ion cyclotron

resonance heating (ICRH) is widely applied to both magnetic confinement fusion [1–5] and high-power electric propulsion [6,7]. The advantages of ICRE over electron cyclotron resonance heating (ECRH) and neutral beam

^{*} Corresponding author.E-mail address: cjxiao@pku.edu.cn (C. Xiao).

injection (NBI) are the low cost of the radio-frequency (RF) source and the ability to directly energize ions [8]. The challenge for ICRE is to increase the efficiency of energy conversion between RF waves and plasmas [9]. Since ICRE involves cyclotron resonance processes, it is necessary to use kinetic methods such as conventional particle-in-cell (PIC) simulations and solving the Boltzmann equation, requiring huge computation and memory [10–15]. The hybrid simulation incorporating of adiabatic electrons and PIC ions provides a viable solution for both a substantial reduction in computation and the inclusion of cyclotron resonance effects. Ilin et al. used a hybrid PIC-MCC (Monte-Carlo Collision) model with adiabatic electron approximation to study ICRE in high-power electric propulsion [11, 16, 17]. However, Ilin et al. did not consider electron collisions and artificially set the electron temperature as a constant. Ion-electron collisions increase the electron temperature proportional to the electrostatic (ES) field which affects the ICRE processes, plasma confinement, and propulsion efficiency. Thus, we add the MCC of electrons to the models of Ilin et al. [11, 16, 17] and develop the HYPIC program able to study the collisional effects of electron on ICRE. We have carefully verified the HYPIC program and given a detailed example of ICRE in magnetic mirror [2, 5]. The advantages of the HYPIC program are the inclusion of (1) the ion kinetic effects, (2) ES and electromagnetic (EM) effects, (3) the collisional effects of ions and electrons, and (4) with a small computation, e.g., the example given in Section 3 consuming about 20 h by one thread. The HYPIC program can be used to fast simulate the antenna-plasma interactions and the ICRE processes in linear devices, such as high-power electric propulsion, magnetic mirror, and field-reversed-configuration (FRC), etc.

This paper is organized as follows. Section 2 presents the simulation model including the governing equations, numerical methods and benchmarks. The applications of HYPIC and a detail example are presented in Section 3. In Section 4, we summarize and discuss.

2. Simulation model

2.1. Governing equations

We use a hybrid EM PIC-MCC model that the equation of motion of ions is solved directly with the adiabatic electron approximation, and the collisions of electrons and ions are solved through the MCC method [18]. The total electric field \mathbf{E} is decomposed into the ES field \mathbf{E}_s and the induced electric field \mathbf{E}_{rf} , i.e., $\mathbf{E} = \mathbf{E}_s + \mathbf{E}_{rf}$. The ES field \mathbf{E}_s can be obtained from the Boltzmann distribution. The induced electric field \mathbf{E}_{rf} , on the other hand, is obtained by solving Maxwell's equations in frequency domain. Details are provided below.

The equation of motion of ions solved in HYPIC is

$$m \frac{d\mathbf{v}}{dt} = q\mathbf{E} + q\mathbf{v} \times \mathbf{B}_0 + \mathbf{F}_c, \quad (1)$$

where the magnetic field contains only the background magnetic field \mathbf{B}_0 since the induced magnetic field is much smaller than the background magnetic field. Solving Ampere's law yields the background magnetic field

$$\nabla \times \mathbf{B}_0 = \mu \mathbf{J}_c, \quad (2)$$

where μ is the permeability and \mathbf{J}_c is the current density of coils [19]. The change of momentum \mathbf{F}_c due to collisions is solved by the MCC method. Four types of collisions are considered, including ion-ion (i-i), ion-electron (i-e), electron-electron (e-e), and electron-ion (e-i) collisions. The adiabatic electron approximation assuming the mass of electron $m_e = 0$ is applied, then the equation of motion of electrons becomes

$$\mathbf{E}_s = T_e \frac{\nabla n_e}{n_e} + \mathbf{u}_e \times \mathbf{B}_0, \quad (3)$$

where n_e , T_e , \mathbf{u}_e are the electron density, electron temperature, and fluid

velocity of electrons, respectively. In the direction parallel to the magnetic field, the Hall term (the second term on the right-hand side of the equation (3) is equal to 0. In the direction perpendicular to the magnetic field, both strong and weak, order of magnitude estimation yields that the pressure gradient term (the first term on the right-hand side of the equation (2) is much larger than the Hall term. For example, by choosing the electron temperature $T_e = 100$ eV, radial plasma radius $r_p = 0.1$ m, perpendicular diffusion coefficient $D_{\perp} \approx 3$ m²/s and magnetic field $B_0 = 0.4$ T, we have $u_{e\perp} = D_{\perp}/r_p = 30$ m/s, and $\nabla_{\perp} p_e / e n_e = T_e / r_p = 10^3$ V/m > $u_{e\perp} B_0 = 12$ V/m. Therefore, the Hall term can be neglected either perpendicular or parallel to the direction of the magnetic field and then the equation (3) can be simplified to

$$\mathbf{E}_s = T_e \frac{\nabla n_e}{n_e}. \quad (4)$$

Macroparticle, an aggregate of N_m real particles (charge and mass), is usually used in PIC simulations. Because the macroparticle number N_m is canceled out in equation (4) under the adiabatic electron approximation, we can use the real ion mass and charge in the equation (2). Therefore, the adiabatic electron approximation not only eliminates the numerical instability caused by electrons, but also avoids the numerical error caused by large N_m when calculating the electrostatic field. However, we still need to determine the macroparticle number N_m to obtain plasma density and power consumption. The N_m is calculated by $N_m = \frac{1}{N_p} = \int \int \int n_{i0}(r, z) r dr d\theta dz$, where $n_{i0}(r, z)$ is the initial plasma density distribution and N_p is the number of ions at the initial time. The ES field is proportional to the electron temperature according to equation (4). The evolution of the electron temperature T_e is expressed by equation

$$\frac{dT_e}{dt} = \nu_{eq}(T_i - T_e), \quad (5)$$

with the equilibration frequency of temperature ν_{eq} [28]. Here we obtain the evolution of the electron temperature T_e by the MCC (collisions associated with electrons) instead of solving equation (5) directly. At the initial moment, we give equal numbers of electrons and ions, after which the velocities of electron change due to collisions (the electron positions not evolving). The electron temperature T_e with unit of eV at any instant can be calculated from the mean kinetic energies of all electrons, i.e., $T_e = 2E_{ke}/3$. We assume that the electron temperature transports fast enough so that the uniform electron temperature can be adopted.

The Maxwell's equations in the frequency domain in the plasma region is

$$\nabla(\nabla \cdot \mathbf{E}_{rf}) - \nabla^2 \mathbf{E}_{rf} - \frac{\omega^2}{c^2} \overset{\longleftrightarrow}{\epsilon} \cdot \mathbf{E}_{rf} = i\omega \mu_0 \mathbf{J}_a. \quad (6)$$

In the vacuum region, with simplification of $\nabla \cdot \mathbf{E}_{rf} = 0$, we have

$$-\nabla^2 \mathbf{E}_{rf} - \frac{\omega^2}{c^2} \epsilon_0 \mathbf{E}_{rf} = i\omega \mu_0 \mathbf{J}_a, \quad (7)$$

where \mathbf{J}_a is the antenna current density and the plasma dielectric tensor $\overset{\longleftrightarrow}{\epsilon}$ [20, 21] in the coordinate system of local magnetic field is given by

$$\overset{\longleftrightarrow}{\epsilon} = \begin{bmatrix} K_{\perp} & -iK_{\phi} & 0 \\ iK_{\phi} & K_{\perp} & 0 \\ 0 & 0 & K_{\parallel} \end{bmatrix}. \quad (8)$$

In the cylindrical coordinate system with axisymmetric background magnetic field $\mathbf{B}_0 = B_0 r \mathbf{e}_r + B_0 z \mathbf{e}_z$, the dielectric tensor becomes

$$\overleftrightarrow{\epsilon} = \begin{bmatrix} \frac{B_{0z}^2 K_{\perp}}{B_0^2} + \frac{B_{0r}^2 K_{\parallel}}{B_0^2} & -\frac{B_{0z}}{B_0} i K_{\phi} & \frac{B_{0z} B_{0r}}{B_0^2} (K_{\parallel} - K_{\perp}) \\ i K_{\phi} \frac{B_{0z}}{B_0} & K_{\perp} & -i K_{\phi} \frac{B_{0r}}{B_0} \\ \frac{B_{0z} B_{0r}}{B_0^2} (K_{\parallel} - K_{\perp}) & i \frac{B_{0r}}{B_0} K_{\phi} & \frac{B_{0z}^2}{B_0^2} K_{\parallel} + \frac{B_{0r}^2}{B_0^2} K_{\perp} \end{bmatrix}. \quad (9)$$

The components of the dielectric tensor in the collisional cold plasma limit [22] are

$$K_{\perp} = 1 - \sum_{l=i,e} \frac{\tilde{\omega}_{pl}^2}{\omega^2 - \omega_{cl}^2},$$

$$K_{\phi} = \sum_{l=i,e} \frac{\tilde{\omega}_{pl}^2 \tilde{\omega}_{cl}}{\omega(\omega^2 - \tilde{\omega}_{cl}^2)},$$

$$K_{\parallel} = 1 - \sum_{l=i,e} \frac{\tilde{\omega}_{pl}^2}{\omega^2},$$

with the electron and ion plasma species $l = e, i$, the modified Langmuir oscillation frequency $\tilde{\omega}_{pl} = \sqrt{q_l^2 n_l / (\varepsilon_0 m_l)}$, the modified cyclotron frequency $\tilde{\omega}_{cl} = q_l B_0 / m_l^{\nu}$, the modified mass $m_l^{\nu} = m_l(1 + i \frac{\nu_l}{\omega})$, the actual real mass m_l , the charge q_l and the effective collision frequency ν_l . The electron collision frequency is given by $\nu_e = \nu_{ei} + \nu_{en}$, with the electron-ion collision frequency $\nu_{ei} = 2.9 \times 10^{-12} \ln \Lambda n_e T_e^{-\frac{3}{2}}$, the electron-neutral collision frequency $\nu_{en} = \sigma_{en} n_n \sqrt{\frac{8 q_e T_e}{\pi m_e}}$ and the cross section σ_{en} [23,24]. The ion collision frequency is given by $\nu_i = \nu_{ie} + \nu_{in}$, with the ion-electron collision frequency $\nu_{ie} = 4.8 \times 10^{-14} Z^4 (m_i/m_p)^{-\frac{1}{2}} n_i \ln \Lambda T_i^{-\frac{3}{2}}$, the ion-neutral collision frequency $\nu_{in} = \sigma_{in} n_n \sqrt{\frac{8 q_i T_i}{\pi m_i}}$, the charge state Z , the proton mass m_p and the cross section σ_{in} [23,25]. Since the cold plasma approximation cannot consider the nonlocal effects, the Doppler shift and the temperature anisotropy, we will update it to a kinetic plasma model [22,26,27] in the next version. In order to save computational resource, we use the finite-difference frequency-domain (FDFD) instead of the finite-difference time-domain (FDTD) methods used in the PHD v1.1 program [28]. By the Fourier transform in time and azimuth, we have $f(r, \theta, z, t) = \sum_{m=-\infty}^{+\infty} f(r, z) e^{im\theta - i\omega t} e_{\theta}$ ($f = E_{rf}, J_a$).

The governing equations of the HYPIC program are summarized as

$$\left\{ \begin{array}{l} m \frac{dv}{dt} = qE + qv \times \mathbf{B}_0 + \mathbf{F}_c \\ n_e = n_i \\ \mathbf{E}_s = T_e \frac{\nabla n_e}{n_e} \\ \frac{dT_e}{dt} = \nu_{eq}(T_i - T_e) \\ \nabla(\nabla \cdot \mathbf{E}_{rf}) - \nabla^2 \mathbf{E}_{rf} - \frac{\omega^2}{c^2} \overleftrightarrow{\epsilon} \cdot \mathbf{E}_{rf} = i\omega \mu_0 \mathbf{J}_a \text{ in plasma} \quad - \nabla^2 \mathbf{E}_{rf} - \frac{\omega^2}{c^2} \overleftrightarrow{\epsilon} \cdot \mathbf{E}_{rf} = i\omega \mu_0 \mathbf{J}_a \text{ in vacuum.} \end{array} \right. \quad (10)$$

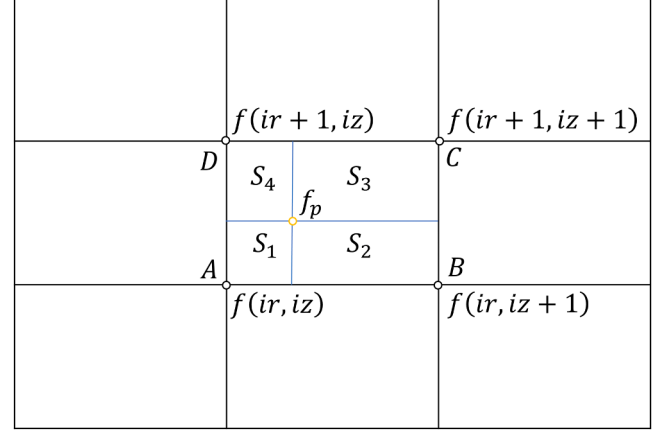


Fig. 1. The PIC bilinear interpolation interpretation, i.e., area s_1, s_2, s_3, s_4 to grid point C, D, A, B respectively.

2.2. Numerical method

The equation of motion (1) are solved in a three-dimensional (3D) Cartesian coordinate system by 4-stage Runge–Kutta (RK4) method [29]. In PIC simulations, since particles are defined in continuum space in both position and velocity and fields are defined on grids, the interaction of particles with fields occurs through linear interpolation scheme [10]. Here we consider azimuthal mode number $m = 0$, thus a 2D (r, z) interpolation, usually called area weighting, can be performed in

$$f_p = \frac{s_3}{s} f(ir, iz) + \frac{s_4}{s} f(ir, iz+1) + \frac{s_1}{s} f(ir+1, iz+1) + \frac{s_2}{s} f(ir+1, iz), \quad (11)$$

where s_1, s_2, s_3, s_4 are the area of the rectangle enclosed by the particle and the neighboring grid points respectively shown in Fig. 1. The area of a grid is $s = s_1 + s_2 + s_3 + s_4 = dr \times dz$.

When finding the particle density n_i , integrating the particle sources to grids is actually the inverse process of interpolation with same coefficients. To suppress numerical dispersion and filter short waves, we smooth the density by averaging over neighboring grids

$$n_i(ir_0, iz_0) = \frac{1}{(2N_{sm} + 1)(4N_{sm} + 1)} \sum_{ir=ir_0-N_{sm}}^{ir_0+N_{sm}} \sum_{iz=iz_0-2N_{sm}}^{iz_0+2N_{sm}} n_i(ir, iz). \quad (12)$$

Smoothing are performed twice in the HYPIC program, with the smoothing parameter N_{sm} taken as 2 and 3, respectively. For particle in-

jection, we generate an initial position distribution of ions satisfying a Gaussian distribution and an initial velocity distribution satisfying a Maxwellian distribution by random numbers. When N_s particles run out of the boundary, the information of these N_s particles is thrown away. At the

Table 1
Default parameter settings.

Parameters	Value
atomic mass number	1 (hydrogen ion)
Number of ions N_p	10^5
Radio frequency f	13.56 MHz
Radial grids N_r	101
Axial grids N_z	101
Initial electron temperature T_{e0}	3 eV
Initial ion temperature T_{i0}	3 eV
Radial boundary of the plasma r_p	0.07 m
macroparticle number N_m	3.2×10^{11}

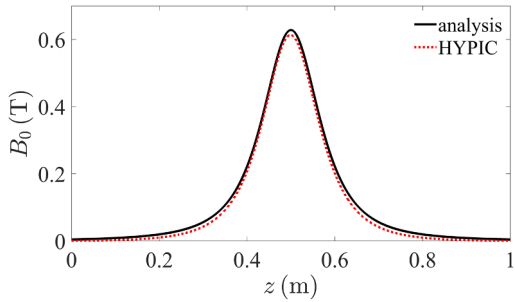


Fig. 2. The axial magnetic field generated by coils, where the black solid line is the analytical solution of the ideal coil and the red dashed line is the result of the HYPIC program.

next time step, new N_s particles will be injected, satisfying a Gaussian distribution for position and a Maxwellian distribution for velocity.

We use the MCC method proposed by Nanbu [18], based on the idea of grouping small-angle binary collisions in plasmas into a unique binary collision with a large scattering angle. Thus, the time step can be increased and the computational time can be greatly reduced. Since it is described carefully enough in reference [18], we will not repeat it.

We use the Yee grid [30] to discretize the fluctuation equations (6–7). Quantities not on the grids are averaged over neighboring grids. The final discretized equations can be written in the form of a system of linear equations and solved by matrix inversion. The HYPIC program solves for 3D (r, θ, z) EM field distributions excited by single-loop antennas [31], helical antennas [32], half-turn antennas [5,9], and Nagoya antennas [33] in non-uniform magnetic fields and non-uniform plasma. Usually the plasma density and electron temperature are slowly varying with time, and thus we can solve the equations (6–7) once every 10 RF cycles to save computational resources. In fact, the EM module in HYPIC and in PHD v2.0 [34] is the same.

Introducing the magnetic vector potential \mathbf{A} ,

$$\mathbf{B}_0 = \nabla \times \mathbf{A}, \quad (13)$$

the equation (2) becomes

$$\nabla(\nabla \cdot \mathbf{A}) - \nabla^2 \mathbf{A} = \mu \mathbf{J}_c. \quad (14)$$

Considering the magnetic field generated by the coils in the cylindrical coordinate system, i.e., $\mathbf{J}_c = J_\theta \mathbf{e}_\theta$, one has

$$-\left(\frac{\partial^2 A_\theta}{\partial r^2} + \frac{\partial^2 A_\theta}{\partial z^2} + \frac{1}{r} \frac{\partial A_\theta}{\partial r} - \frac{A_\theta}{r^2} \right) = \mu J_\theta. \quad (15)$$

The equation (15) are discretized by central differences and solved by Gaussian iteration. The iteration format without ferromagnetic medium is

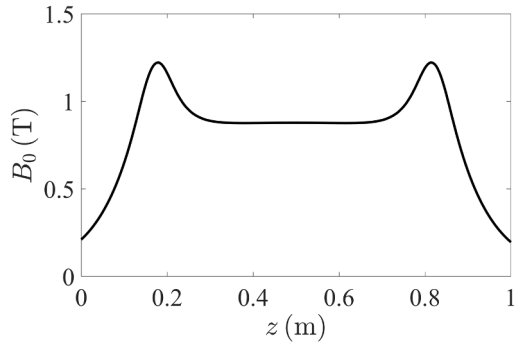


Fig. 3. Distribution of magnetic field with axial position at $r = 0.02$ m.

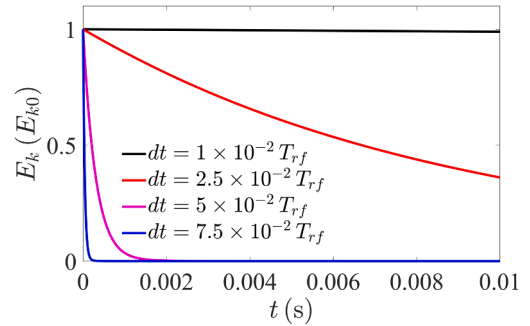


Fig. 4. The evolution of the mean kinetic energy of all particles E_k over time, where only the Lorentz force is considered and E_{k0} is the initial mean kinetic energy.

$$\begin{aligned} & \left(\frac{2}{\Delta r^2} + \frac{2}{\Delta z^2} + \frac{1}{r^2} \right) A_\theta(ir, iz) = \mu_0 J_\theta + \\ & \left(\frac{A_\theta(ir+1, iz) + A_\theta(ir-1, iz)}{\Delta r^2} + \frac{A_\theta(ir, iz+1) + A_\theta(ir, iz-1)}{\Delta z^2} \right. \\ & \left. + \frac{A_\theta(ir+1, iz) - A_\theta(ir-1, iz)}{2r\Delta r} \right). \end{aligned} \quad (16)$$

For the case with a ferromagnetic medium, the iteration format can be found in reference [19]. Finally, we can obtain the magnetic field by

$$B = -\frac{\partial A_\theta}{\partial z} \mathbf{e}_r + \left(\frac{\partial A_\theta}{\partial r} + \frac{A_\theta}{r} \right) \mathbf{e}_z. \quad (17)$$

The ES field, magnetic field and density are calculated and interpolated in 2D cylindrical coordinate system (r, z). The motion of the particles is calculated in 3D Cartesian coordinate system (x, y, z) and the induced electric field is calculated in 3D cylindrical coordinate system (r, θ, z). Taken together, HYPIC is a 2D (r, z) EM PIC-MCC program able to fast simulate the antenna-plasma interactions and ICRE processes in the cylindrical coordinate system. In addition, the HYPIC program has a good modularity for the background magnetic field, the motion of the particles, the RF antenna-plasma interaction, and the MCC, so that the user can easily use one or more of these functions. Unless otherwise specified, the parameters in this paper are listed in Table 1.

2.3. Benchmarks

For the verification of the background magnetic field, we compare the numerical results with the analytical solution. The problem to be solved is the axial distribution of the magnetic field generated by an ideal coil, with analytical solution

$$B_0(z) = \frac{\mu_0 I_0 R_c^2}{2(R_c^2 + (z - Z_c)^2)^{\frac{3}{2}}}, \quad (18)$$

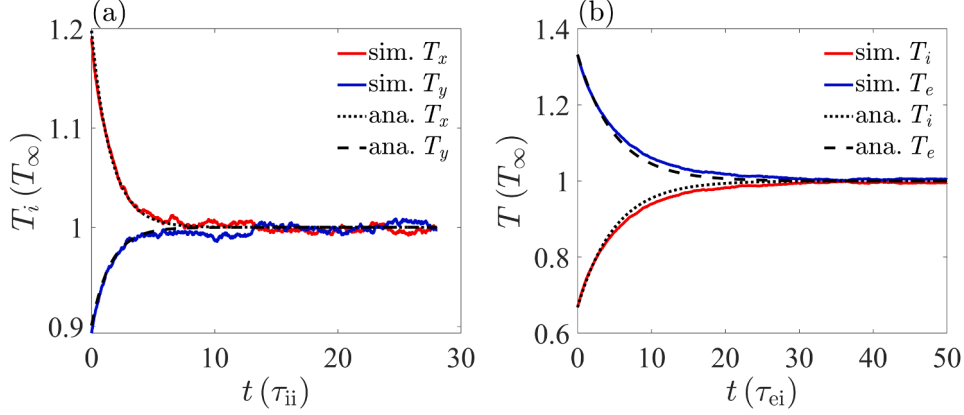


Fig. 5. The (a) i-i collision and (b) e-i collision relaxation process.

where the radius and axial position of the coil are $R_c = 0.1$ m, $Z_c = 0.5$ m, and the current of the coil is $I_0 = 10^5$ A. In HYPIC calculation, we set a coil with radial width 0.01 m and the axial width 0.02 m. The computational region is $r \in [0, 0.3]$ m, $z \in [-0.5, 1.5]$ m and the number of grids is $N_r \times N_z = 301 \times 2001$. Fig. 2 shows the results calculated by the HYPIC program and the analytical solution for the ideal coil, and it can be seen that they are in general agreement, with a maximum difference of 2.4%. This small difference may be due to the non-ideal coil in HYPIC calculation. Therefore, the background magnetic field module in the HYPIC program is reliable.

The solution of the motion equation (1) and the conservation of energy are verified next. The evolution of the mean kinetic energy in the system with time is discussed here by considering only the Lorentz force (magnetic field) and ignoring the electric field force and collisions. Since the Lorentz force does no work, the kinetic energy of the particles should be conserved. To avoid the loss of ions, we adopt a periodic boundary condition in the axial boundaries and a reflection boundary condition in the radial boundary. The magnetic field of magnetic mirror used here is shown in Fig. 3. The number of particles is $N_p = 10^4$. We set the initial velocities $v_{x0} = 10v_{y0} = 10v_{z0}$ in order to make the particles as constrained as possible by the magnetic mirror. Fig. 4 shows the evolution of the mean kinetic energy of all particles E_k over time, and it can be seen that the smaller the time step, the better the energy conservation. In particular, the energy loss rate ($1 - E_k/E_{k0}$) at $t = 0.01$ s is 1.07% in the case of $dt = 10^{-2} T_{rf}$, where the RF cycle is $T_{rf} = 1/f$. Our calculations

are usually within 0.01 s, so we default to $dt = 10^{-2} T_{rf}$. In addition, although the RK4 method is in explicit form, it is dissipative in nature.

The MCC module is then verified. Two questions are discussed here, including ion velocity reaching isotropy from anisotropy through i-i collisions, and ions and electrons reaching thermal equilibrium through collisions. We set the initial temperature $T_x = 1.3T_y = 1.3T_z$ in the first question (i-i collisions). The total ion temperature is ($=\frac{1}{3}T_x + \frac{2}{3}T_y$), and the analytical solution $\Delta T (= T_x - T_y)$ [18,35] is

$$\Delta T_{xy} = (\Delta T_{xy})_0 \exp\left(-\frac{8}{5\sqrt{2}} \frac{t}{\tau_0}\right), \quad (19)$$

where the collision time (reference time) $\tau_0 = 8\pi\sqrt{2m_i\varepsilon_0^2 T_i^{3/2}}/(n_i e^4 \ln \Lambda)$, T_i in eV, the density of the ions n_i , and the initial temperature difference $(\Delta T_{xy})_0$. The collision time step is taken as $dt_{mcc} = 10^{-2}\tau_0$. Fig. 5(a) shows that the simulation results are in good agreement with the analytical solution.

Then, we take the initial temperature $T_{e0} = 2T_{i0}$ in the second question (e-i collision relaxation process) with e-i, i-e, e-e, i-i collisions considered. In order to accelerate the relaxation process, the electron mass is taken to be $m_e = m_i/4$. According to the reference [35], the temperature difference ΔT_{ei} ($T_e - T_i$) is solved analytically as

$$\Delta T_{ei} = (\Delta T_{ei})_0 \exp(-2\nu_{eq}t), \quad (20)$$

with $\nu_{eq} = 8\nu_0 m_e (1 + m_e T_i / (m_i T_e))^{-\frac{3}{2}} / (3m_i \sqrt{\pi})$, $\nu_0 =$

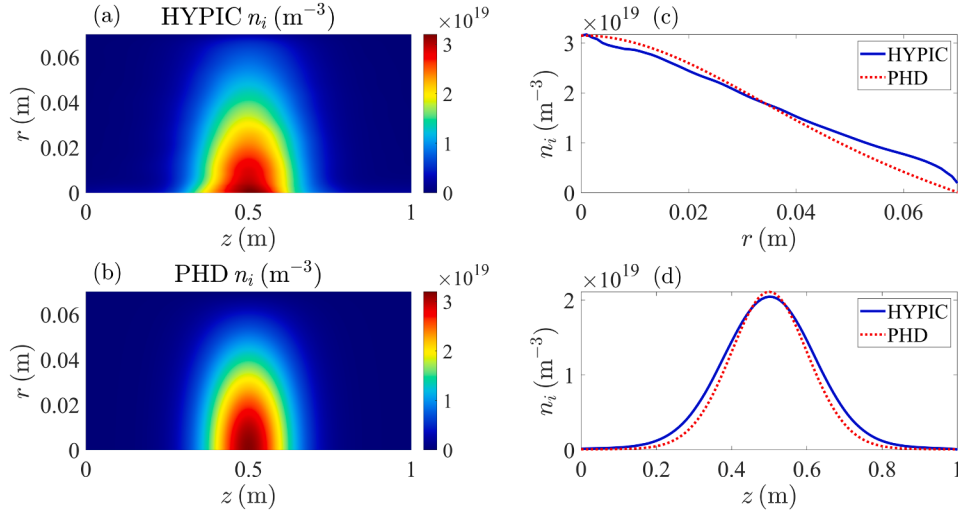


Fig. 6. Steady-state ion density distributions simulated by (a) the HYPIC program and (b) the PHD program with $B_0 = 0$. (c) The radial ion density at $z = 0.5$ m and (d) the axial the ion density at $r = 0.03$ m.

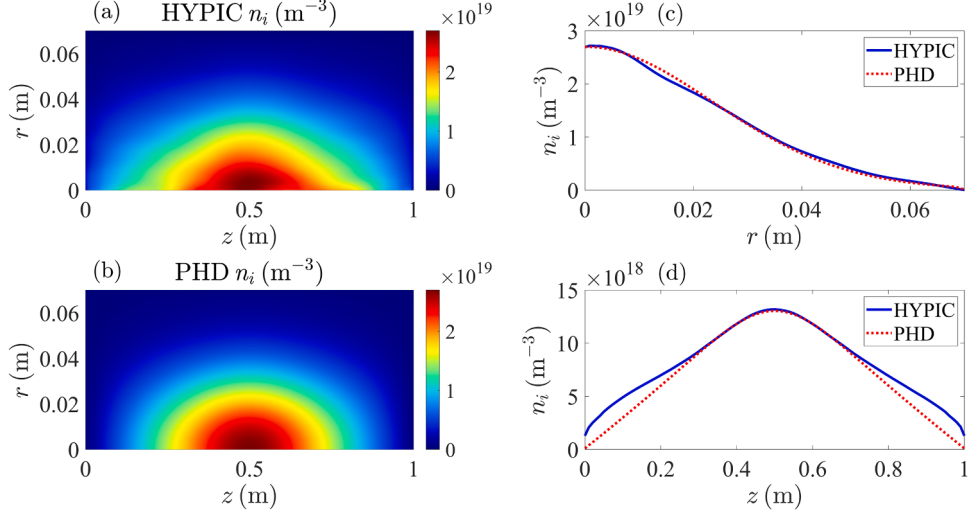


Fig. 7. Steady-state ion density distributions simulated by (a) the HYPIC program and (b) the PHD program with $B_0 = 0.4$ T. (c) The radial ion density at $z = 0.5$ m and (d) the axial the ion density at $r = 0.03$ m.

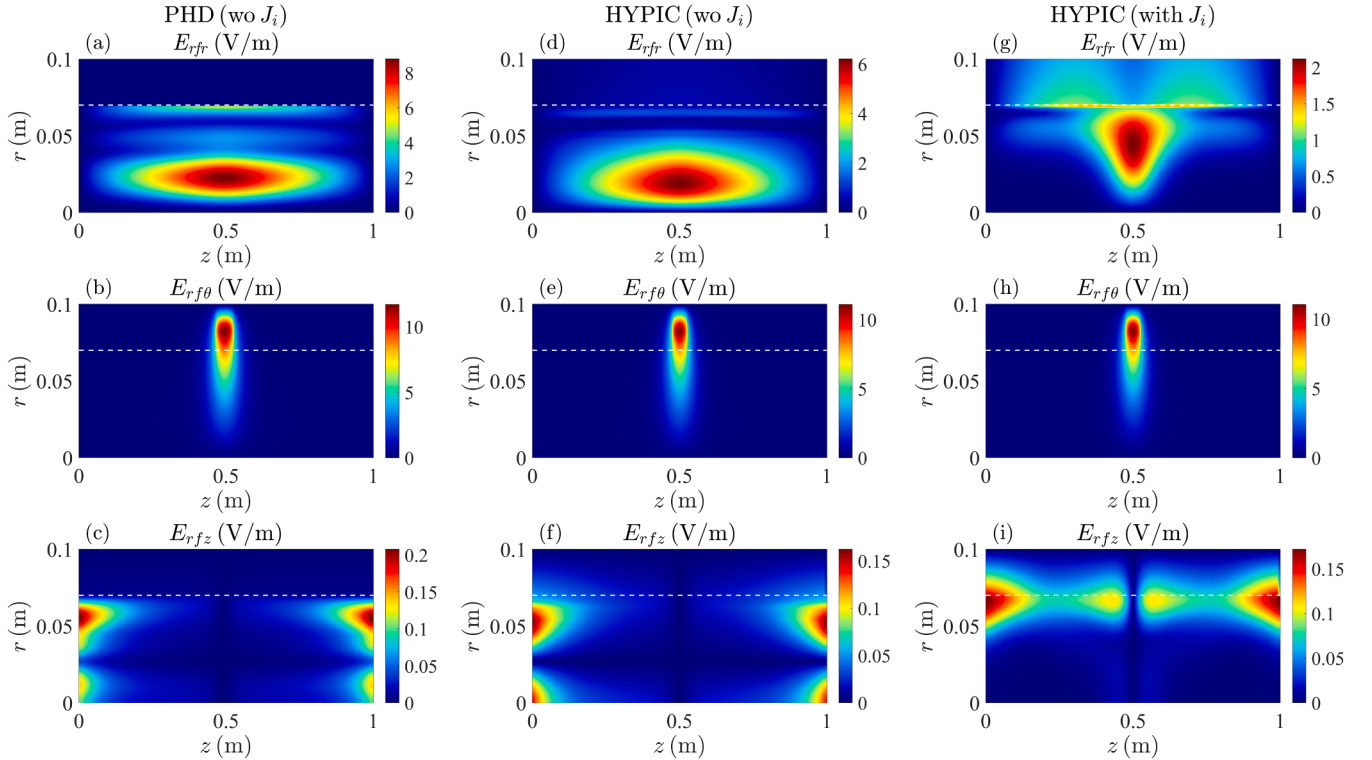


Fig. 8. The (a) radial electric field E_{rfr} , (b) azimuthal electric field $E_{rf\theta}$, (c) axial electric field E_{rfz} calculated by PHD. The (d) radial electric field E_{rfr} , (e) azimuthal electric field $E_{rf\theta}$, (f) axial electric field E_{rfz} calculated by HYPIC without J_i . The (g) radial electric field E_{rfr} , (h) azimuthal electric field $E_{rf\theta}$, (i) axial electric field E_{rfz} calculated by HYPIC with J_i .

$n_i e^4 \ln \Lambda / (8\pi \sqrt{2m_e} \epsilon_0^2 T_e^{3/2})$. The collision time step is taken as $dt_{mcc} = 10^{-2}/\nu_0$. Fig. 5(b) shows the comparison of the simulation with the analysis, indicating the convergence times of the two results being close. In fact, these two questions and the simulation results in Fig. 5 are similar to those in reference [19]. Overall, the HYPIC simulation are in good agreement with the analysis, indicating the MCC module being verified.

Benchmarks are necessary when analytical solutions are not available, and typically they represent more realistic tests. The HYPIC transport module is verified by the magnetohydrodynamic (MHD) program PHD v1.1 [28]. The physical model of the PHD program, focusing

on the helicon discharge processes, is the system of fluid equations (transport and ionization) coupled with Maxwell's equations (wave propagation and power deposition). The similarity of HYPIC and PHD is that both study the diffusion of magnetized plasma and the interaction of the RF antenna with the plasma. Unlike PHD using the fluid transport model, HYPIC employs the PIC model under the adiabatic electron approximation, which includes the kinetic effects of ions. In addition, the interaction of ion current with RF waves is added in the HYPIC EM module. The problem discussed is to solve for the steady-state plasma density given the plasma source $S = S_0 \exp\left(-\frac{r^2}{2r_w^2}\right) \exp\left(-\frac{(z-z_c)^2}{2z_w^2}\right)$, where

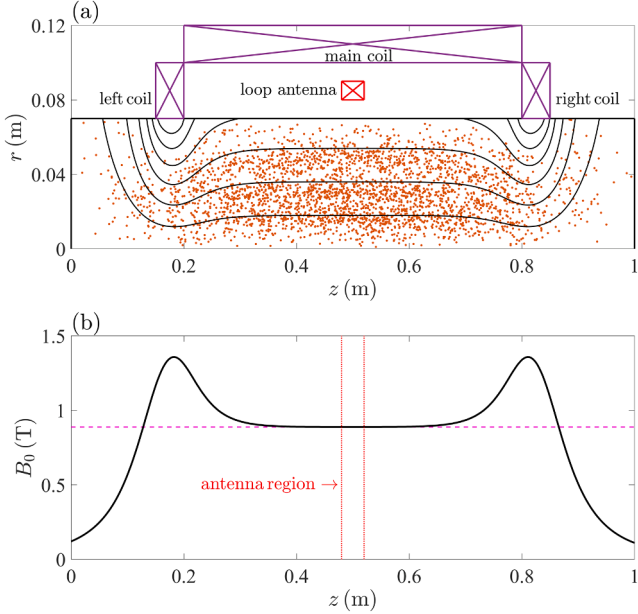


Fig. 9. (a) Schematic of the simulated configuration, where the coils generating the background magnetic field are marked in purple. The thick black solid lines are the plasma boundary, and only the magnetic lines (thin black solid lines) in the plasma region are shown. The ions are represented by the brown dots. (b) Variation of the magnetic field at $r = 0.02$ m, with the horizontal dashed line representing the resonant magnetic field.

radial width, axial width and axial center position are $r_w = 0.025$ m, $z_w = 0.1$ m, $z_c = 0.5$ m respectively. The effects of ES fields, magnetic fields and collisions are considered. The transport model for the PHD program [28] is

$$\frac{\partial n}{\partial t} + \nabla \cdot \Gamma = S, \quad (21)$$

$$n = n_i = n_e, \quad (22)$$

$$\Gamma = -D_\perp \nabla_\perp n e_\perp - D_\parallel \nabla_\parallel n e_\parallel. \quad (23)$$

The electron temperature is fixed at $T_e = 3$ eV.

The case of $B_0 = 0$ with $S_0 = 1.68 \times 10^{25} \text{ m}^{-3}\text{s}^{-1}$ is discussed first. Fig. 6 shows the steady-state density n_i obtained by the HYPIC and PHD simulations. The plasma density distributions and values are broadly similar for both. The density of HYPIC is slightly wider than that of PHD, probably due to the smoothness in HYPIC.

The case of $B_0 = 0.4$ T with $S_0 = 1.61 \times 10^{23} \text{ m}^{-3}\text{s}^{-1}$ is then discussed. The plasma density distributions and values are also similar for HYPIC and PHD, shown in Fig. 7. The difference between the two may also be caused by the smoothness in HYPIC.

Overall, HYPIC and PHD give similar results, verifying HYPIC's transport module.

Finally, the EM modules in HYPIC and PHD v1.1 [28] are compared. Unlike the FDFD in HYPIC, PHD uses FDTD method and ignores the electron current. The induced electric field E_{rf} generated by a single loop antenna is calculated. The position of the antenna is $(r_a, z_a) = (0.08, 0.5)$ m with the radial width 0.01 m and axial width 0.04 m. The plasma density is Gaussian distributed with $n_e = n_{e0} \exp\left(-\frac{r^2}{2r_w^2}\right) \exp\left(-\frac{(z-z_c)^2}{2z_w^2}\right)$, where $r_w = 0.02$ m, $z_w = 0.2$ m, $z_c = 0.5$ m, $n_{e0} = 10^{19} \text{ m}^{-3}$.

The radius of the plasma is $r_p = 0.07$ m. The ideal conductor boundary conditions are used for both axial and radial boundaries. The uniform background magnetic field is taken, i.e., $B_0 = B_0 e_z$, $B_0 = 0.4$ T, with $f = 6$ MHz. The amplitude of E_{rf} obtained by HYPIC and PHD is shown in Fig. 8. It can be seen that the radial electric fields E_{rf} are both centrally

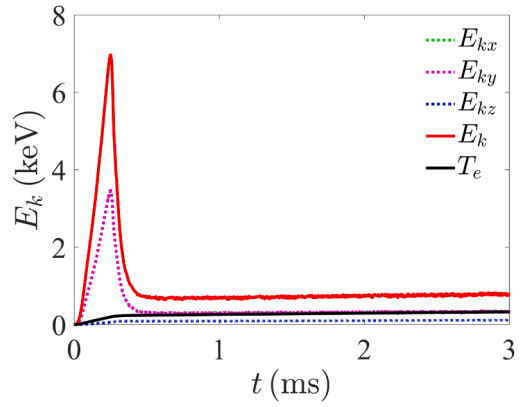


Fig. 10. Evolution of the mean kinetic energy of ions and electron temperature with time.

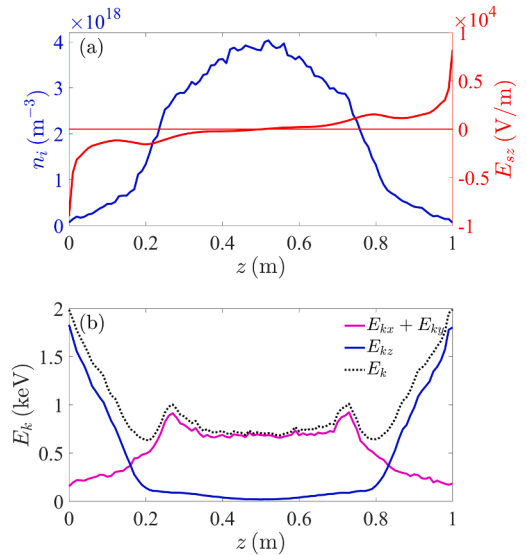


Fig. 11. Distribution of the mean (a) ion density n_i , axial ES field E_{sz} and (b) kinetic energy of ions E_k along the axial position at $t = 3$ ms.

peaked, but E_{rf} in PHD is narrower than that in HYPIC, probably due to HYPIC optimization ($\nabla \cdot E_{rf} = 0$) in the vacuum region. The azimuthal and axial electric field distributions of HYPIC and PHD are very close to each other both in terms of values and shapes. Comparison of the HYPIC results with and without the ion current shows that the ion current cannot be neglected near the ion cyclotron frequency. Overall, the HYPIC's EM module is reliable.

To summarize, we have carried out detailed verifications and benchmarks of HYPIC and confirmed that the HYPIC program is reliable.

3. Application

Setting different conditions such as background magnetic field, antenna, plasma density, configuration, etc., the HYPIC program can be used to fast simulate the antenna-plasma interactions and ICRE processes in a variety of linear devices, such as magnetic mirrors, high-power electric propulsion, and FRC. The ICRE in magnetic mirrors as an example is shown next.

3.1. Simulation configuration

We have designed a magnetic mirror shown in Fig. 9, consisting of three coils, the main coil, the left coil, and the right coil. The main coil generates a relatively uniform background magnetic field, and the left and

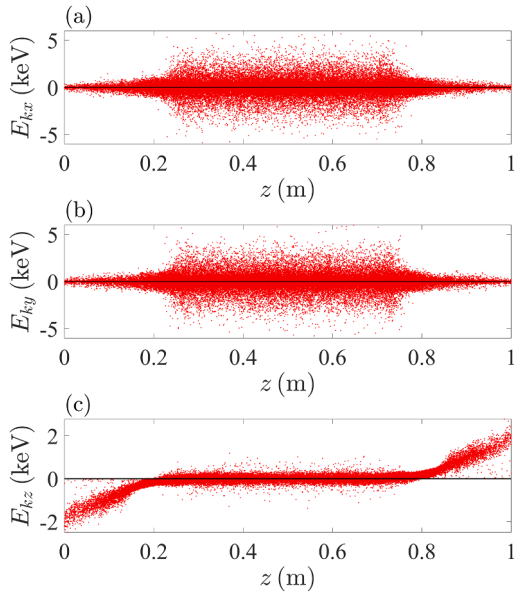


Fig. 12. The ion kinetic energy distribution (a) E_{kx} , (b) E_{ky} and (c) E_{kz} along the axial direction at $t = 3$ ms, with positive and negative representing their velocity directions.

right coils generate the stronger confining magnetic field, shown in Fig. 9 (a). The position coordinates (r_1 , r_2 , z_1 , z_2) of the main, left and right coils are (0.1, 0.12, 0.2, 0.8) m, (0.07, 0.1, 0.15, 0.2) m, (0.07, 0.1, 0.8, 0.85) m, and the numbers of ampere-turns are 4.50×10^5 A, 1.31×10^5 A, 1.31×10^5 A, respectively. The magnetic lines are shown in Fig. 9(a) and the magnitude of the magnetic field is shown in Fig. 9(b). The coordinates (r_1 , r_2 , z_1 , z_2) of the single loop antenna are (0.08, 0.09, 0.48, 0.52) m. The uniform background magnetic field near the antenna is intended to ensure high energy coupling efficiency [9]. The RF frequency is $f = 13.56$ MHz and the current amplitude is $I_{rf} = 10$ A.

3.2. Simulation results

Fig. 10 shows the evolution of the mean kinetic energy of ions E_k and electron temperature T_e with time, indicating that the ion kinetic energy increases firstly and then decreases and gradually stabilizes. Another important information of $E_{kx} \approx E_{ky} \gg E_{kz}$ indicates that the ICRE mainly increases the cyclotron kinetic energy ($E_{kx} + E_{ky}$). It is difficult for ions to reach thermal equilibrium ($E_{kx} \approx E_{ky} \approx E_{kz}$) through collisions, and that is why we usually call it ICRE (without sufficient collision) instead of ICRR (with sufficient collision). The electron temperature is significantly less than the ion kinetic energy, indicating that electrons and ions also have difficulty in reaching thermal equilibrium through collisions.

Fig. 11 shows the distribution of n_i , E_{sz} and E_k along the axial position at $t = 3$ ms. $E_{kx} + E_{ky} \gg E_{kz}$ near the antenna ($0.3 \text{ m} < z < 0.7 \text{ m}$) also indicates that the ICRE mainly increases the cyclotron kinetic energy. At $z < 0.2 \text{ m}$ and $z > 0.8 \text{ m}$, the cyclotron kinetic energy decreases while the parallel kinetic energy increases rapidly due to two reasons of (1) the axial ES field E_{sz} accelerating the ions shown in Fig. 11(a), and (2) the evanescent magnetic field converting the cyclotron kinetic energy ($E_{kx} + E_{ky}$) to the parallel kinetic energy E_{kz} due to the conservation of magnetic moments. Fig. 11(b) shows two bumps of the cyclotron kinetic energy round $z \sim 0.25 \text{ m}$ and $z \sim 0.75 \text{ m}$. This is due to the fact that the ions are generated from the center ($z \sim 0.5 \text{ m}$) and gain effective acceleration in the region of uniform magnetic field ($0.25 \text{ m} < z < 0.75 \text{ m}$), accompanied by an increase in the cyclotron kinetic energy. Ions with high cyclotron kinetic energy are reflected by the magnetic mirror and confined in the region of $0.25 \text{ m} < z < 0.75 \text{ m}$. Only ions with low cyclotron kinetic energy will enter the loss cone, accounting for the low cyclotron kinetic energy in the region of $0.2 \text{ m} < z < 0.25 \text{ m}$ and $0.75 \text{ m} < z < 0.8 \text{ m}$.

Fig. 12 shows the kinetic energy distribution of the ions along the axial direction at $t = 3$ ms. The E_{kx} and E_{ky} have a good symmetry about $E_k = 0$. The kinetic energy is widely distributed in the region of the magnetic mirror confinement ($0.3 < z < 0.7 \text{ m}$), with many energetic ions. In the region of $z < 0.2 \text{ m}$ and $z > 0.8 \text{ m}$, most of the ions have axial velocities pointing toward the boundary.

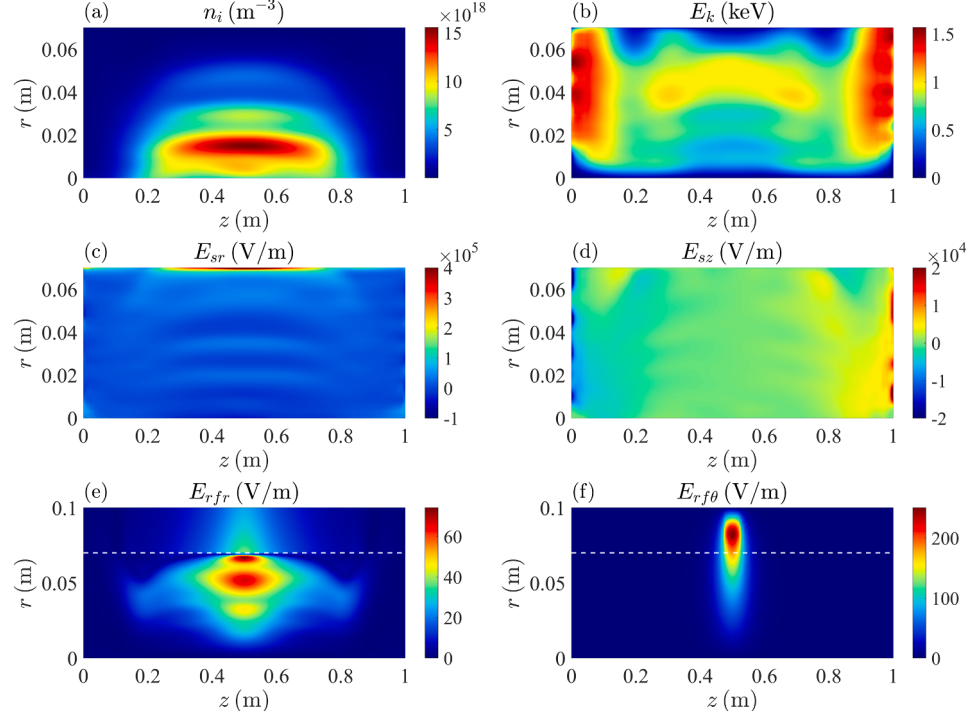


Fig. 13. Two-dimensional distribution of (a) ion density n_i , (b) ion kinetic energy E_k , (c) radial ES field E_{sr} , (d) axial ES field E_{sz} , (e) radial induced electric field E_{rfr} , and (f) azimuthal induced electric field $E_{rf\theta}$ $t = 3$ ms.

Fig. 13 shows the 2D (r, z) distribution of ion density n_i , ion kinetic energy E_k , radial ES field E_{sr} , axial ES field E_{sz} , radial induced electric field E_{rfr} , and azimuthal induced electric field $E_{rf\theta}$ at $t = 3$ ms. The density is concentrated in the region of the magnetic mirror confinement, where the ions are accelerated up to about 3 keV. The radial ES field has large values mainly at the radial boundary, where the plasma density gradient is large. Both radial and axial ES fields have large values near the plasma boundary. After careful analysis, it is found that the phase difference of time evolution between the radial ion velocities v_r and the radial induced electric field E_{rfr} is close to 0. Thus, it can be obtained that the E_{rfr} dominates the ICRE here. Unlike the azimuthal induced electric field $E_{rf\theta}$ accelerating ions [9], the E_{rfr} can also accelerate the ions. In fact, the effective ICRE is expected to solve the end-loss problem of the magnetic mirror fusion. The methods are that ICRE can rapidly increase the cyclotron kinetic energy when the ions entered the loss cone by collisions, leading the ions out of the loss cone and into the confinement state. The study of confinement and energization in magnetic mirror is not the subject of this work and will be discussed in detail elsewhere.

4. Conclusion and discussion

To summarize, we have developed a 2D (r, z) EM PIC-MCC program in the cylindrical coordinate system, named HYPIC, able to fast simulate the antenna-plasma interactions and the ICRE processes in linear devices such as high-power electric propulsion, magnetic mirror, and FRC, etc. We provide a detailed verification of each module and an example of the ICRE in magnetic mirror. The main advantages of the HYPIC program are inclusion of (1) the kinetic effects of ions, (2) the ES and EM effects, (3) the collisions between ions and electrons, and (4) with a small computation, e.g., the example given in Section 3 consuming about 20 h by one thread. Although the collisional effects on the electron temperature is considered, the spatial distribution of the electron temperature and the heating effect of RF waves are not considered. The electron temperature evolution equation will be solved in the next work.

CRediT authorship contribution statement

Mingyang Wu: Writing – review & editing, Writing – original draft, Validation, Software, Methodology, Investigation, Formal analysis, Data curation, Conceptualization. **Andong Xu:** Software, Methodology, Investigation, Formal analysis, Data curation. **Chijie Xiao:** Funding acquisition, Project administration, Supervision.

Declaration of competing interest

The authors declare that they have no known competing financial interests or personal relationships that could have appeared to influence the work reported in this paper.

Data availability

Data will be made available on request.

Acknowledgments

We would like to acknowledge Ting Gao for useful discussions. This work was supported by the National Key Research and Development Program of China(No. 2022YFA1604600).

Supplementary materials

Supplementary material associated with this article can be found, in

the online version, at doi:10.1016/j.cpc.2024.109207.

References

- [1] M. Tuszeński, Field reversed configurations, Nucl. Fus. 28 (1988) 008.
- [2] T. Tamano, Tandem mirror experiments in GAMMA 10, Phys. Plasmas 2 (1995) 2321.
- [3] D.F.H. Start, J. Jacquinot, V. Bergeaud, V.P. Bhatnagar, G.A. Cottrell, S. Clement, L. G. Eriksson, A. Fasoli, A. Gondhalekar, C. Gormezano, et al., D-T fusion with ion cyclotron resonance heating in the JET tokamak, Phys. Rev. Lett. 80 (1998) 4681.
- [4] A.H. Glasser, S. Cohen, Ion and electron acceleration in the field-reversed configuration with an odd-parity rotating magnetic field, Phys. Plasmas 9 (2002) 2093.
- [5] M. Liu, H.S. Yi, G.H. Zhu, Z.D. Yang, M.N. Lin, X. Sun, Ion cyclotron resonant heating in the central cell of the Keda Mirror with AXisymmetry (KMAX), Phys. Plasmas 25 (2018) 6.
- [6] A.V. Arefiev, B.N. Breizman, Theoretical components of the VASIMR plasma propulsion concept, Phys. Plasmas 11 (2004) 2942.
- [7] Z.Y. Yang, W. Fan, X. Han, C. Tan, The resonance between electromagnetic field and electrons in the helicon plasma source of magnetoplasmoid rocket engine, Front. Phys. 11 (2023) 1182960.
- [8] J.P. Freidberg, *Plasma Physics and Fusion Energy*. Cambridge university press, 2008.
- [9] M. Wu, C. Xiao, X. Wang, C. Tan, T. Xu, R. He, R. Yuan, A. Xu, A new configuration for high power propulsion plasmas driven by ion cyclotron resonance energization, Phys. Plasmas 29 (2022) 023508.
- [10] C.K. Birdsall, Particle-in-cell charged-particle simulations, plus Monte Carlo collisions with neutral atoms, PIC-MCC, IEEE Trans. Plasma Sci. 19 (1991) 65.
- [11] A. Ilin, F.C. Díaz, J. Squire, B. Breizman, M. Carter, *Particle simulations of plasma heating in VASIMR[C]*, in: AIAA/ASME/SAE/ASEE Joint Propulsion Conference & Exhibit, 2000.
- [12] S. Pécou, S. Heuraux, R. Koch, G. Leclert, Numerical modeling of the coupling of an ICRH antenna with a plasma with self-consistent antenna currents, Comput. Phys. Commun. 146 (2002) 166.
- [13] J.P. Verboncoeur, Particle simulation of plasmas: review and advances, Plasma Phys. Control Fus. 47 (2005) A231.
- [14] D. Tskhakaya, K. Matyash, R. Schneider, F. Taccogna, The Particle-In-Cell Method, Contrib. Plasma Phys. 47 (2007) 563.
- [15] M. Brambilla, R. Bilato, Advances in numerical simulations of ion cyclotron heating of non-Maxwellian plasmas, Nucl. Fus. 49 (2009) 085004.
- [16] A.V. Ilin, F.R.C. Diaz, J.P. Squire, M.D. Carter, Monte-Carlo particle dynamics in a variable specific impulse magnetoplasmoid rocket, Fus. Technol. 35 (1999) 330.
- [17] A. Ilin, F.Chang Diaz, J. Squire, M. Carter, *Plasma heating simulation in the VASIMR system[C]*, in: 43rd AIAA Aerospace Sciences Meeting and Exhibit, 2005.
- [18] K. Nanbu, Theory of cumulative small-angle collisions in plasmas, Phys. Rev. E 55 (1997) 4642.
- [19] N. Li, Y. Liu, C. Liu, M. Wu, An integrated fluid simulation platform on Hall thruster plasmas, AIP. Adv. 12 (2022).
- [20] T.H. Stix, *Waves in Plasmas*. Springer Science & Business Media, 1992.
- [21] H.S. Xie, D. Banerjee, Y.K. Bai, H.Y. Zhao, J.C. Li, BORAY: a ray tracing code for various magnetized plasma configurations, Comput. Phys. Commun. 276 (2022) 10.
- [22] A. Ilin, F.Chang Diaz, J. Squire, A. Tarditi, M. Carter, *Simulation of ICRF plasma heating in the VASIMR experiment[C]*, in: 42nd AIAA Aerospace Sciences Meeting and Exhibit, 2004.
- [23] J.D. Huba, *NRL Plasma Formulary*. Naval Research Laboratory, 1998.
- [24] M.Y. Wu, C.J. Xiao, Y. Liu, X.Y. Yang, X.G. Wang, C. Tan, Q. Sun, Effects of magnetic field on electron power absorption in helicon fluid simulation, Plasma Sci. Technol. 23 (2021) 085002.
- [25] R. Stewart, P. Vitello, D. Graves, E. Jaeger, L. Berry, Plasma uniformity in high-density inductively coupled plasma tools, Plasma Sources Sci. Technol. 4 (1995) 36.
- [26] P.L. Colestock, R. Kashuba, The theory of mode conversion and wave damping near the ion cyclotron frequency, Nucl. Fus. 23 (1983) 763.
- [27] A.V. Ilin, F.R.C. Diaz, J.P. Squire, A.G. Tarditi, M.D. Carter, Improved simulation of the ICRF waves in the VASIMR plasma, Comput. Phys. Commun. 164 (2004) 251.
- [28] W. Mingyang, X. Chijie, W. Xiaogang, L. Yue, X. Min, T. Chang, X. Tianchao, Y. Xiuming, H. Renchuan, X. Andong, Relationship of mode transitions and standing waves in helicon plasmas, Plasma Sci. Technol. 24 (2022) 055002.
- [29] U.M. Ascher, L.R. Petzold, *Computer Methods For Ordinary Differential Equations and Differential-Algebraic Equations*. Siam, 1998.
- [30] K. Yee, Numerical solution of initial boundary value problems involving Maxwell's equations in isotropic media, IEEE Trans. Antennas. Propag. 14 (1966) 302.
- [31] N. Jiwari, T. Fukasawa, H. Kawakami, H. Shindo, Y. Horiike, Helicon wave plasma reactor employing single-loop antenna, J. Vacuum Sci. Technol. A: Vacuum, Surf. Films 12 (1994) 1322.
- [32] T. Shoji, Y. Sakawa, S. Nakazawa, K. Kadota, T. Sato, Plasma production by helicon waves, Plasma Sources Sci. Technol. 2 (1993) 5.
- [33] F.F. Chen, RF production of high density plasmas for accelerators, Laser Particle Beams 7 (1989) 551.
- [34] A. Xu, M. Wu, C. Xiao, T. Xu, Z. Zhang, R. Yuan, *A Numerical Comparison on Helicon Discharges with Different Antennas*, Submitted.
- [35] T. Takizuka, H. Abe, Binary collision model for plasma simulation with a particle code, J. Comput. Phys. 25 (1977) 205.